

Lidar and Camera Self-Calibration using Cost Volume Network

Xudong Lv*, Boya Wang*, Dong Ye, and Shuo Wang

I. INTRODUCTION

In the past few years, research on autonomous driving technology has developed rapidly. The working environment of autonomous driving is very complex and highly dynamic. There is still a long way to go to achieve a fully autonomous driving. To ensure the accurate and stable perception of the surrounding environment, autonomous cars are usually equipped with a series of different sensors, such as cameras, lidar, millimeter-wave radar, GPS/IMU inertial navigation system, etc. Currently, no single sensor can ensure stable perception in all scenarios. To overcome the limitations and defects of different sensors, complementary information provided by multiple sensors, and multi-sensor fusion techniques are used to reduce the uncertainty of environmental perception. The basis of multi-sensor fusion is accurate calibration between various sensors, that is, accurate estimation of the relative rigid body transformation between sensors. Our main research content in this paper is the calibration between LiDAR and camera, which are common on-board sensors of autonomous vehicles and autonomous navigation robots. LiDAR point cloud and camera image belong to heterogeneous data. Compared with homologous data (such as multi-camera calibration), calibration between heterogeneous data acquisition devices is more difficult. We need to determine the accurate correspondence between data collected by different sensors. For LiDAR and camera, we need to accurately extract the 2D-3D matching relationship between the 3D point cloud of LiDAR and the 2D pixels of the corresponding image.

Some early calibration work utilized specific artificial markers, such as checkerboard and special calibration plates, to calibrate LiDAR and cameras. Most marker-based calibration algorithms are time-consuming, laborious, and off-line which is not suitable for self-driving cars. In the process of vehicle operation, the position between sensors will drift slightly with the running time, so the sensor needs to be re-calibrated after every period of operation to eliminate the accumulated calibration error caused by the drift. During the operation of the vehicle, the position between the sensors will drift slightly with the running time. Thus, after a period of operation, the sensors need to be re-calibrated again to eliminate the accumulated error caused by drift. Some recent calibration methods for LiDAR and cameras focus on fully automatic

and target-less online self-calibration. However, most online self-calibration methods have strict requirements on calibration scenarios, and the calibration accuracy is not as high as offline calibration algorithms based on markers. Some researchers try to apply deep learning to the calibration tasks, using convolutional neural networks to predict the 6-DOF rigid body transformation between the two sensors. These methods directly fuse the features extracted from the image and the point cloud, without considering the correlation between these two features. In this article, we propose a new method for predicting extrinsic calibration parameters of LiDAR and camera. More specifically, our contribution can be concluded as follows:

(1) Compared with other CNN-based methods that concatenate the features of RGB image and decalibrated depth image with the following convolutional layers, we construct a cost volume to describe the matching costs between these two features for feature matching.

(2) The training data is expanded by adding a random deviation to the ground truth extrinsic calibration matrix. Instead of predicting the calibration parameters between LiDAR and camera directly, our proposed network predicts the random deviation.

(3) We use the quaternion as the ground truth during supervised training. In addition to smooth L1-Loss between the predicted calibration and ground truth, an additional point cloud loss is presented.

II. RELATED WORK

Recently, the research of various scene understanding tasks is promoted by exploiting multi-modal sensors. Effective fusion of these multi-modal data relies heavily on accurate registration of the various sensors. Therefore, extrinsic calibration of sensors is a vital step for the scene understanding research, especially the sensors with different modalities. In this paper, we focus on the extrinsic calibration of LiDAR and camera with the assumption that the intrinsic parameter of sensors has been aligned already. With the association of point cloud and RGB image, the purpose of LiDAR-Camera extrinsic calibration is the estimation of the 6-DOF rigid-body transformation between these two sensors. The 3D-2D registration between LiDAR and camera has three main solutions:

(a) Place specific markers (such as checkerboard) in the scene, and extract the features of markers to build cost function. The calibration accuracy depends on the matching points and the optimization method.

Corresponding author: Shuo Wang

* contributed equally to this work

Xudong Lv, Boya Wang, Dong Ye, and Shuo Wang are with School of Instrumentation Science and Engineering, Harbin Institute of Technology, Harbin 150001, China (email: 15B901019@hit.edu.cn; 19B901034@stu.hit.edu.cn; yedong@hit.edu.cn; 15B901018@hit.edu.cn)

(b) Without the markers, we can obtain the calibration parameters by maximizing the correlation of LiDAR reflectivity with camera intensity or depth discontinuity with the image edge in a target-less way.

(c) Apply CNN to predict the extrinsic calibration parameter between LiDAR and camera.

A. Target-based methods

Li et al. [1] designed a right-angled triangular checkerboard and established the constraints equations by using the invisible intersection points of the slice plane from Laser rangefinder (LRF) with the edges of the checkerboard. This method minimizes the algebraic errors between the measured intersections and their corresponding projection on the image plane of the camera to calibrate the extrinsic parameters. Geige et al. [2] realize calibration by multiple printed checkerboard patterns on the walls and floors. Define a camera as a reference, all checkerboards in the target image are assigned to the nearest position in the reference image given the expectation. The rotation ambiguity problem is solved by minimizing the angular projection error of each matched checkerboard. Polygon calibration plates are also applied, Park et al. [3] estimate the corresponding 3D points by LiDAR scans on the edges of adjacent polygonal planar boards. The vertex of the board is estimated to be the intersection of the two adjacent projected edges of the polygon planar board due to the length of the edges of the calibration board is known. The 2D vertical lines detected from the RGB image and the 3D vertical lines estimated from the LiDAR point cloud are regarded as the correspondences of calibration.

A new rough-calibrated 3D marker is proposed in [4] as a calibration plate, which can be detected in camera images and LiDAR scans. [5] employs hollow circles as the calibration target to find the center of the circle in 2D image data and 3D LiDAR data respectively. The optimal transformation was obtained under the condition of no rotation and the corresponding centers of mass are matched. Pusztai et al. [6] adopt the carton of known size as the calibration plate to detect the surface of the box. An iterative process is employed to refine the plane of the box into a set of points. After matching with the 2D image by rotation transformation, the fitting error is minimized by iteration. Besides the corners and edges of the calibration plate, Jiao et al. [7] propose a novel calibration method that considers the normal vector of the target plane as another effective feature to figure out the extrinsic calibration parameters. For the simplification of the calibration process, the rotation matrix and translation vector are solved respectively. Mirzaei et al. [8] divide the estimation of the intrinsic parameter of LiDAR and the extrinsic parameter between LiDAR and camera into two least-square sub-problems. Iteratively minimizing a batch nonlinear least-squares cost function can improve the accuracy of initial estimation.

[9] advances a method for extrinsic calibration of cameras and a 3D LRF aided by an additional Inertial Measurement Unit (IMU). The rotation matrix between LRF and camera is determined when the motion observation of the robot and sensor is realized by IMU. Wang et al. [10] develop a new

automatic extrinsic calibration method for 3D LiDAR and panoramic camera using checkerboard. Mishra et al. [11] propose a LiDAR-camera extrinsic estimation algorithm on unmarked plane target, by utilizing Planar Surface Point to Plane and Planar Edge Point to back-projected Plane geometric constraint. During the process of data collection, the calibration plates are placed in different poses in the common field of view of LiDAR and camera. The geometric constraint cost function for calibration is constructed by exploiting the planes and lines detected from LiDAR point clouds and images.

B. Target-less methods

Scaramuzz et al. [12] present a self-calibration method for 3D LRF and camera extrinsic calibration in a natural scene. Given a group of corresponding point pairs, Perspective-N-Point (PnP) algorithm and nonlinear optimization are exploited for extrinsic calibration. Tamas et al. [13] propose a nonlinear explicit correspondence-less calibration method that regards the calibration problem as a 2D-3D registration of a common LiDAR-camera region. Minimal information like depth data and shape of regions are applied to construct the registration non-linear system, which provides the calibration parameters of LiDAR-camera directly. Furthermore, Tamas et al. [14] advance a new method of estimating the extrinsic calibration of 3D LiDAR and Omnidirectional Cameras. Without the usage of 2D-3D corresponding points or complex similarity measurement, this method depends on a set of corresponding regions, and regress the pose by solving a small nonlinear system of equations. Pandey et al. [15] adopt the effective correlation coefficient between the surface reflectivity measured by LiDAR and the intensity measured by a camera as one of the parameters of extrinsic calibration function, while the other parameters remain unchanged.

Registering the gradient direction of the data obtained by the two sensors is another target-less method. [16] estimates the extrinsic parameter by minimizing the misalignment of the gradient to realize data registration. Kang et al. [17] employs the projection model-based edge alignment to construct the cost function, taking full advantage of the dense photometric and sparse geometry measurement methods. Among them, many-to-many correspondence of the edges is expressed using the Gaussian Mixture Model (GMM). The calibration parameters are estimated by minimizing the cost function for evaluating correspondence of the edges between two sensor measurements. Besides, a rough to fine strategy is proposed to improve the stability of the algorithm by gradually reducing the standard deviation of GMM.

C. CNN-based methods

RegNet [18] transforms the three conventional calibration steps (feature extraction, feature matching, and global regression) into a real-time Convolutional Neural Network (CNN) to deduce the 6-DOF of extrinsic parameters between LiDAR and camera. CalibNet [19] proposes a self-monitoring deep network that automatically estimates the 6-DOF rigid-body transformations between 3D lidar and 2D camera in real-time. During the training, the calibration parameters are not

used as the supervision directly. Instead, end-to-end training is performed by maximizing the geometric and photometric consistency between the input image and the point cloud. SOIC [20] exploits semantic information to calibrate and transforms the initialization problem into the PNP problem of the semantic centroid. Due to the 3D semantic centroid of the point cloud and the 2D semantic centroid of the image cannot match accurately, a matching constraint cost function based on the semantic elements of the image and the LiDAR point cloud is also proposed. The optimal calibration parameter is obtained by minimizing the cost function. Zhu et al. [21] propose an online calibration system that automatically calculates the optimal rigid-body motion transformation between two sensors by maximizing the mutual information of their perceived data without adjusting the environment Settings. By formulating the calibration as an optimization problem with semantic features, the temporally synchronized LiDAR and camera are registered in real-time.

III. METHOD

Our goal is to apply the LiDAR point cloud and the RGB image to realize the self-calibration of the two sensors without markers. Similar to [18], [19], we leverage deep convolutional neural networks to predict the 6-DOF extrinsic calibration between LiDAR and camera. The workflow block diagram of our proposed method is shown in Figure 1. In the following sections, we illustrate our proposed calibration method, including the acquisition of training data, the design of the network and the loss function, subsequent refinement, and the details of training.

A. Train Data Collection

The performance of deep learning methods depends on the quality and quantity of data presented to them. For LiDAR-camera calibration, the data we need is pairs of images and LiDAR scans accompanied with calibration ground truth. Commonly, the extrinsic calibration parameters between LiDAR and cameras are provided by using some complex calibration algorithm [2]. For the most dataset, sensors are calibrated before collecting data, which means the frames and LiDAR scans in each sequence share the same registration parameters. Besides, after the sensors are installed, the relative position of the sensors will not change significantly. Therefore, the difference between the extrinsic parameters of the LiDAR and the camera is very small, which cannot meet the needs of training data.

To solve the insufficiency of training data, we add a random deviation ΔT within a reasonable range to the extrinsic calibration matrix of LiDAR and camera. In this paper, we define the extrinsic parameter T_{LC} as the Euclidean transformation from the LiDAR coordinate to the camera coordinate. After adding the random parameter ΔT to T_{LC} , the initial extrinsic $T_{init} = \Delta T \cdot T_{LC}$ is obtained. By randomly changing the deviation value, we can acquire a large amount of training data.

Given initial extrinsic T_{init} and camera intrinsic K , we can generate the LiDAR-image by projecting each 3D point cloud

$P_i = [X_i \ Y_i \ Z_i] \in \mathbb{R}^3$ from the LiDAR scan onto a virtual image plane with a 2D pixel coordinate $p_i = [u_i \ v_i] \in \mathbb{R}^2$. The projection process is expressed as follows:

$$\begin{aligned} Z_i^{init} \cdot \hat{p}_i &= Z_i^{init} [u_i \ v_i \ 1]^T \\ &= K [R_{init} | t_{init}] \hat{P}_i \end{aligned} \quad (1)$$

$$\begin{aligned} &= K [R_{init} | t_{init}] [X_i \ Y_i \ Z_i \ 1]^T \\ T_{init} &= \begin{bmatrix} R_{init} & t_{init} \\ 0 & 1 \end{bmatrix} \end{aligned} \quad (2)$$

where \hat{P}_i and \hat{p}_i represent the homogeneous coordinates of P_i and p_i . By using a Z-buffer method, the LiDAR-image is computed to determine the visibility of points along the same projection line, where every pixel (u_i, v_i) preserves the depth value Z_i^{init} of a 3D point P_i on camera coordinate.

If the pixel in the image has no corresponding projection point cloud, the value for that pixel is set to zero. The sparse depth map obtained by projecting the LiDAR point cloud with T_{init} is shown in Figure 2. Compared with the RGB image, the LiDAR point cloud is relatively sparse, so the projected depth map is also sparse. To solve the issue of depth map sparseness, we sample the original RGB image and sparse depth map. For instance, the Max pooling approach can be applied to obtain the depth map that is smaller in scale but much denser than the original image.

For the ground truth ΔT mentioned above, we use the form of a homogeneous matrix to present. The transformation matrix consists of a 3×3 rotation matrix R_{gt} and a 3×1 translation vector t_{gt} :

$$\Delta T = \begin{bmatrix} R_{gt} & t_{gt} \\ 0 & 1 \end{bmatrix} \quad (3)$$

To reduce the output parameters of the network, Euler angles, lie algebras, or quaternions can take the place of the rotation matrix. [18] makes a contrast test on Euler Angle and quaternion, and the experimental results show that the training result using quaternion as ground truth is superior to Euler Angle. Therefore, the quaternion is regarded as ground truth in this paper.

B. Network Architecture

The proposed calibration network is mainly composed of three parts: feature extraction network, feature matching layer and feature global aggregation. Since the parameters in each part are differentiable, CNN can be trained end-to-end. The overall structure framework of the calibration network is shown in Figure. 3. We will describe the structure and function of each part of this section.

1) *Feature Extraction Network*: The feature extraction network consists of 2 symmetric branches, extracting the features of the RGB image and LiDAR-image. For the RGB branch, we use a pre-trained ResNet-18 network excluding the full connection layer. Different from [18, 19] decreasing the convolutional layer with half the number of filters at each stage, the depth branch is consistent with the RGB branch. Some modifications are applied to the depth branch on the

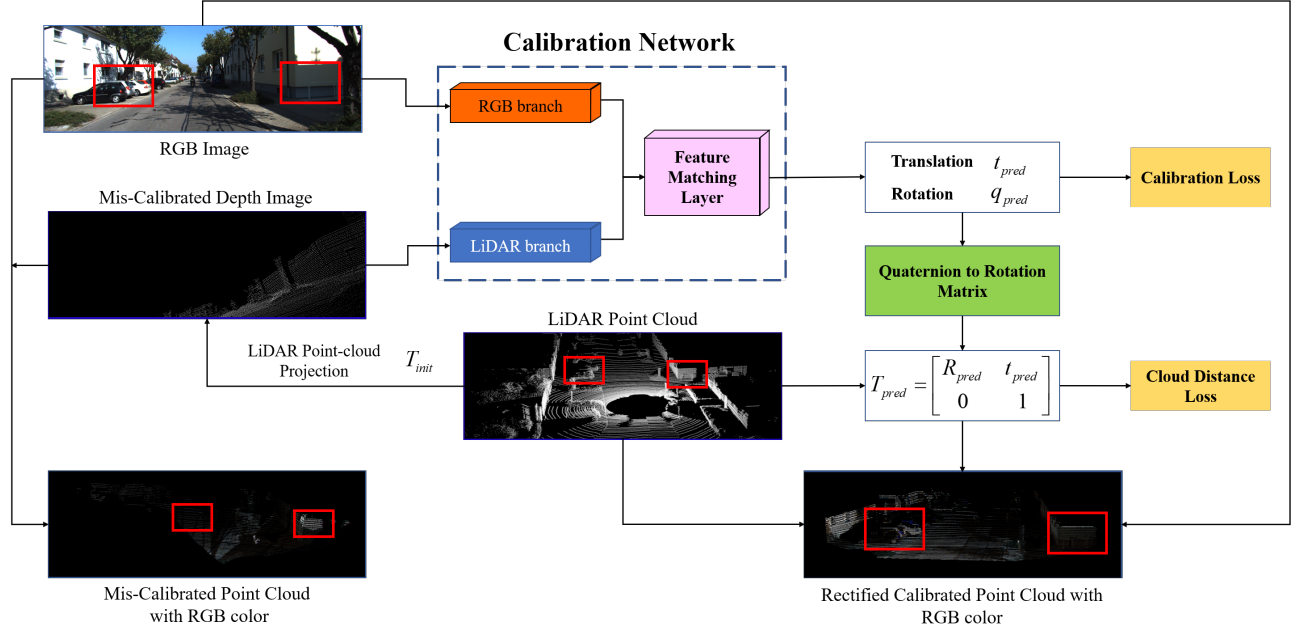


Fig. 1: The workflow of our proposed method for the estimation of the extrinsic calibration parameters between 3D LiDAR and 2D camera. The network takes an RGB image from a calibrated camera and a projected sparse depth image from a mis-calibrated LiDAR as input. The output of the network is a 6-DOF rigid-body transformation T_{pred} that represents the deviation between the initial extrinsic T_{init} and the ground truth extrinsic T_{LC} . As shown, we notice that the 3D structure highlighted using red rectangles fails to project to their 2D counterparts with the mis-calibrated depth image. When using the predicted transformation T_{pred} to revise the T_{init} , we can reconstruct a more consistent and accurate 3D scene structure.



Fig. 2: We deviate from the initial calibration up to 20° in rotation and up to 1.5m in translation from the ground truth calibration. This may lead to the projection of LiDAR points, most of which are outside the field-of-view of the camera, thus it is difficult to establish the corresponding relationship with RGB image.

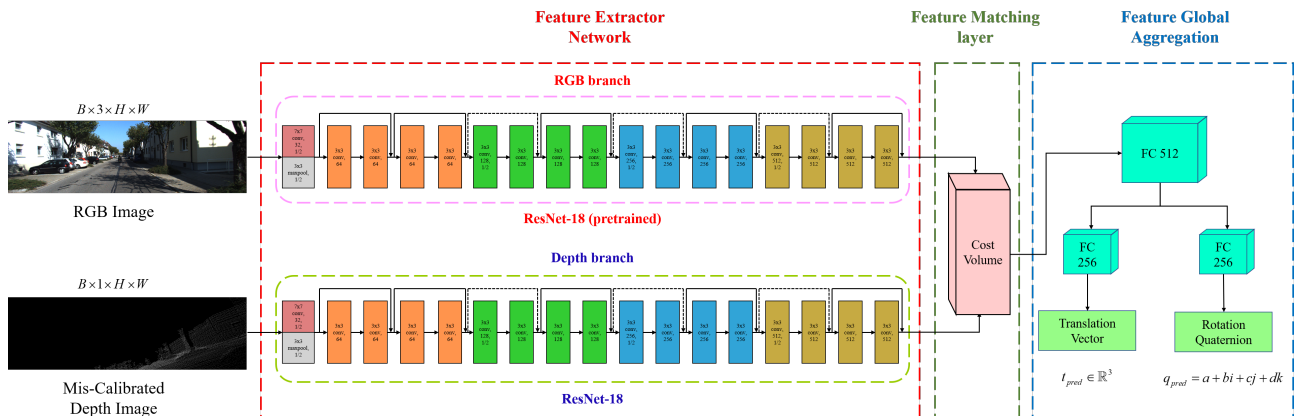


Fig. 3: Network architecture.

basis of the RGB branch: (1) The original activation function RELU (REctified Linear Unit) in ResNet is replaced by leaky RELU. (2) The input channel of the first convolutional layer is changed from three to one.

2) *Feature Matching Layer*: After extracting features from two input modalities, a feature matching layer is adopted to calculate the matching cost for associating a pixel in RGB feature maps x_{rgb} with its corresponding depth feature maps x_{lidar} . Inspired by PWC-Net [22], we take advantage of the correlation layer for feature matching. We define the constructed cost volume as the correlation between x_{rgb} and x_{lidar} that stores the matching cost:

$$cv(p_1, p_2) = \frac{1}{N} (c(x_{rgb}(p_1)))^T c(x_{lidar}(p_2)) \quad (4)$$

where $c(x)$ is the flattened vector of feature maps x , N is the length of the column vector $c(x)$, T is the transpose operator. For the features, we need to compute a local cost volume with a limited range of d pixels, i.e., $|p_1 - p_2|_\infty \leq d$. Since the input feature maps are very small, $1/32$ of the full resolution images, we need to set the value d very small ($d = 2$ in this paper). The dimension of the 3D cost volume cv is $d^2 \times H \times W$, where H and W donate the height and width of feature maps x_{rgb} and x_{lidar} , respectively.

3) *Feature Global Aggregation*: The function of this network is to regress the 6-DOF rigid-body transformation between LiDAR and camera with cost volume features. This network consists of a full connection layer with 512 neurons and two branches with stacked full connection layers representing rotation and translation. The output of the network is a 1×3 translation vector t_{pred} and a 1×4 rotation quaternion q_{pred} .

C. Loss Function

Given an input pair composed of an RGB image I and a LiDAR-image D_{init} , we use two types of loss terms during training: regression loss L_T and point cloud loss L_P .

$$L = \lambda_T L_T + \lambda_P L_P \quad (5)$$

where λ_T and λ_P denotes respective loss weight.

1) *Regression Loss*: For the translation vector t_{pred} , the smooth $L1$ loss is applied. The derivative of $L1$ loss is not unique at zero, which may affect the convergence of training. Compared to $L1$ loss, the smooth $L1$ loss is much smoother due to the usage of the square function near zero. The regression loss of translation vector is defined as:

$$L_t = \begin{cases} 0.5(t_{pred} - t_{gt})^2, & |t_{pred} - t_{gt}| < 1 \\ |t_{pred} - t_{gt}| - 0.5, & |t_{pred} - t_{gt}| > 1 \end{cases} \quad (6)$$

where t_{pred} is the predicted translation vector, t_{gt} is the corresponding ground truth. Regarding the rotation loss L_q , since quaternions are essentially directional information, Euclidean distance cannot accurately describe the difference between the two quaternions. Therefore, we use angular distance to represent the difference between quaternions, as defined below:

$$L_R = D_a(q_{gt} * inv(q_{pred})) \quad (7)$$

$$D_a(m) = atan2(\sqrt{b_m^2 + c_m^2 + d_m^2}, |a_m|) \quad (8)$$

$$atan2(y, x) = \begin{cases} \arctan(\frac{y}{x}) & x > 0 \\ \arctan(\frac{y}{x}) + \pi & y \geq 0, x < 0 \\ \arctan(\frac{y}{x}) - \pi & y < 0, x < 0 \\ \frac{\pi}{2} & y > 0, x = 0 \\ -\frac{\pi}{2} & y < 0, x = 0 \\ \text{undefined} & y = 0, x = 0 \end{cases} \quad (9)$$

where q_{gt} is the ground truth of quaternion, q_{pred} is the prediction, $\{a_m, b_m, c_m, d_m\}$ is four components of a quaternion m , inv is the inverse of a quaternion, $*$ represent the multiplication of two quaternions. For a quaternion $m = a_m + b_m i + c_m j + d_m k$, its inverse is shown as:

$$\begin{aligned} inv(m) &= \frac{\bar{m}}{m^2} = \frac{a_m - b_m i - c_m j - d_m k}{\|m\|^2} \\ &= \frac{a_m - b_m i - c_m j - d_m k}{a_m^2 + b_m^2 + c_m^2 + d_m^2} \end{aligned} \quad (10)$$

where \bar{m} is the conjugate quaternion of m , $\|m\|$ is the length of m . The total regression loss L_T is the combination of translation and rotation loss:

$$L_T = \lambda_t L_t + \lambda_q L_R \quad (11)$$

where λ_t and λ_q denotes respective loss weight.

2) *Point Cloud Loss*: Besides the regression loss, a point cloud constrain is added to the loss function. After transforming the quaternion $q_{pred}(w, x, y, z) = w + xi + yj + zk$ to a rotation matrix R_{pred} , we can obtain the homogeneous matrix T_{pred} :

$$\begin{aligned} R_{pred} &= \begin{bmatrix} 1 - 2y^2 - 2z^2 & 2xy + 2wz & 2xz - 2wy \\ 2xy - 2wz & 1 - 2x^2 - 2z^2 & 2yz + 2wx \\ 2xz + 2wy & 2yz - 2wx & 1 - 2x^2 - 2y^2 \end{bmatrix} \end{aligned} \quad (12)$$

$$T_{pred} = \begin{bmatrix} R_{pred} & t_{pred} \\ 0 & 1 \end{bmatrix} \quad (13)$$

Given a group of LiDAR point cloud $P = \{P_1, P_2, \dots, P_N\}$, $P_i \in \mathbb{R}^3$, the point cloud loss L_P is defined as:

$$L_P = \frac{1}{N} \sum_{i=1}^N \|(\Delta T^{-1} \cdot T_{pred}) P_i\|_2 \quad (14)$$

where N is the number of point clouds, $\|\cdot\|_2$ denotes the $L2$ Normalization.

D. Calibration Inference and Refinement

1) *Extrinsic Calibration Inference*: The extrinsic calibration parameter between the uncalibrated LiDAR and camera can be obtained by combining the predicted results T_{pred} of the calibration network and the initial calibration parameter T_{init} . As long as the parameter T_{init} ensures a certain number of LiDAR points projected on the RGB image, we can guarantee the accuracy of the calibration. The extrinsic calibration parameter is expressed as:

$$\hat{T}_{LC} = T_{pred}^{-1} \cdot T_{init} \quad (15)$$

2) Iterative Refinement:

(a) Single-range Network Iteration

The LiDAR-image exists a great variability according to the random initial calibration parameter T_{init} . As illustrated in Figure 2, some T_{init} bring about that most of the LiDAR point cloud is projected outside the field-of-view of the camera, resulting in only minimal connections between LiDAR and camera. To deal with this problem, the iterative optimization approach is adopted to improve the accuracy of the calibration. We regard the prediction T_{pred} as T_0 , and re-project the LiDAR point cloud with $T_0^{-1} \cdot T_{init}$ to generate a new LiDAR-image including more projected LiDAR points. The new LiDAR-image and RGB image is consisted of input pairs of the calibration network to predict new transformation T_1 . The aforementioned process is iterated n times to get the final extrinsic calibration matrix.

$$\hat{T}_{LC} = (T_0 \cdot T_1 \dots T_n)^{-1} \cdot T_{init} \quad (16)$$

(b) Multi-range Network Iteration

If we want our proposed method has a large mis-calibration, the range of the random deviation ΔT should be set as large as possible. In this paper, we set the deviation range of the translation and rotation to $[-1.5m, 1.5m]$ and $[-20^\circ, 20^\circ]$. The loss function penalizes larger partial derivatives of loss, that is why a large mis-calibration range has more impact on the network than a small one. This results in unsatisfactory calibration results when the random deviation is small or iterative prediction. To compensate for this effect, we train multiple networks on different mis-calibration ranges. According to the illustration in [18], [19], the latter smaller range is determined by the maximum mean absolute error (MAE) of the predicted results after training the network using the former larger range. We choose the same translation and rotation range as [18]: $[-x, x], x = \{1.5m, 1.0m, 0.5m, 0.2m, 0.1m\}$, $[-y, y], y = \{20^\circ, 10^\circ, 5^\circ, 2^\circ, 1^\circ\}$. The accuracy of the iterative prediction can be improved by using the method of multi-range network iterative prediction in place of the single-range network.

3) *Temporal Filtering*: The method we proposed above only uses one frame of the camera and one scan of LiDAR to predict the extrinsic calibration. While in reality, only a few scenes need to calibrate between two sensors in the case of one frame. In an autopilot environment, extrinsic calibration between different sensors may involve more than one frame. This approach yields more reliable results if the network output is analyzed over time using a moving average.

IV. EXPERIMENTS AND DISCUSSION

We evaluate our proposed calibration approach on the KITTI autonomous driving dataset. In this section, we detail the data preprocessing, evaluation metrics, training procedure, and discuss the results of different experiments.

A. Dataset Preparation

We use the odometry branch from the KITTI dataset [23] to verify our proposed algorithm. KITTI Odometry dataset

consists of 21 sequences from different scenarios. Each sequence contains images captured from two color and two grayscale PointGrey Flea2 video cameras, and point clouds from a Velodyne HDL-64E 3D laser scanner. In addition, the dataset also provides calibration parameters between each sensor, among which the calibration parameters between lidar and camera were obtained by [2] as the ground truth of extrinsic calibration parameters in our experiment. In this paper, we only consider the calibration between the LiDAR and the left color camera. Specifically, we used sequences from 01 to 20 for training (39011 frames in total) and sequence 00 for validating (4541 frames in total). The validation dataset is spatially independent of the training dataset, except for a very small subset sequence (about 200 frames), so it can be assumed that the test scenario is not in the training data.

The original dimension of the raw recordings from the KITTI dataset is 1392×512 . After data filtering, image distortion, and cropping, the dimension of the images in the odometry dataset are inconsistent (range from 1224×370 to 1242×376). To satisfy the input requirement of the network that the width and the height of the input data must be a multiple of 32, we apply zero paddings on the original image to 1280×384 . It should be noted that we obtain the sparse depth map by projecting the LiDAR point cloud on the original RGB image and carry out zero paddings to both the RGB and depth images. By doing this, we can ensure the accuracy of input data without changing the camera intrinsic parameter for projection. After padding, a series of data augmentation methods, randomly changing the intensity, contrast, situation, and hue of the RGB image are adopted. The RGB image and the depth image are then randomly mirrored. Since the initial relative pose T_{init} is set randomly, the RGB image and LiDAR point cloud of the same frame were different in each epoch. The number of training dataset could also be increased in a disguised way by taking advantage of this random variable.

B. Evaluation Metrics

The experimental results are analyzed according to the rotation and translation of the calibration parameters. The translation vector is evaluated by the Euclidian distance between the vectors. The absolute error of the translation vector is expressed as follows:

$$E_t = \|t_{pred} - t_{gt}\|_2 \quad (17)$$

where $\|\cdot\|_2$ denotes the 2-norm of a vector. Besides, we also test the absolute error of the translation vector in X, Y, Z directions respectively.

The rotation part is represented by quaternions. Since quaternion represents direction, we use quaternion angle distance to represent the difference between quaternions. The angle error of quaternion can be expressed as follows:

$$E_R = D_a(q_{gt} * inv(q_{pred})) \quad (18)$$

where $D_a(\cdot)$ is the quaternion angle $D_a(\cdot)$ expressed in Equation 8. To test the angle error of the extrinsic rotation matrix on three degrees, we need to transform the rotation

matrix to Euler angles and compute the angle error of Roll, Pitch, and Yaw.

$$R_{pred}^{-1} \cdot R_{gt} = \begin{bmatrix} r_{11} & r_{12} & r_{13} \\ r_{21} & r_{22} & r_{23} \\ r_{31} & r_{32} & r_{33} \end{bmatrix} \quad (19)$$

$$\begin{aligned} E_{yaw} &= \theta_z = \text{atan2}(r_{21}, r_{11}) \\ E_{pitch} &= \theta_y = \text{atan2}(-r_{31}, \sqrt{r_{31}^2 + r_{33}^2}) \\ E_{roll} &= \theta_x = \text{atan2}(r_{32}, r_{33}) \end{aligned} \quad (20)$$

C. Training Details

The depth branch of the network uses Leaky RELU as an activation function with a negative slope of 0.1 as non-linearity. For training the network, we use Adam Optimizer with an initial learning rate $3e^{-4}$. We train our proposed calibration network on two Nvidia GP100 GPU with batch size 120 and total epochs 120. For the multi-range network, it is not necessary to retrain each network from scratch. Instead, a large-range model can be regarded as the pre-trained model for small-range training to speed up the training process. The training epoch of the model with the largest range is set to 120, while the others are set to 50.

D. Results and discussion

1) *Calibration Evaluation:* Figure 4 shows the results of our proposed calibration method on the validation dataset. It can be seen that the larger the miscalibration between initial extrinsic and ground truth, the larger the absolute error. For the rotation part, the error in the Pitch direction is significantly higher than Yaw and roll, and the error in the Roll direction is the smallest. Compared to the rotation, the absolute error of the translation part on three coordinate axes is similar. As shown in Figure 5(c), the LiDAR-image acquired by projecting LiDAR point cloud with the predicted extrinsic parameter \hat{T}_{LC} has some difference with the ground truth LiDAR-image shown in Figure 5(d). The results of the absolute calibration error are described in Table I, our approach achieves a mean square translation error of 17.840cm, a mean translation error of 8.210cm (x, y, z: 11.849cm, 5.169cm, 7.613cm) and a mean quaternion angle error of 1.235°, a mean angle error of 0.480° (roll, pitch, yaw: 0.170°, 0.676°, 0.594°). The execution time of the calibration approach is 24 ms for one network forward pass on an NVIDIA TITAN X GPU.

2) Iterative Refinement:

(a) The evaluation of a single-range network.

By comparing the results illustrated in Figure 4 and Figure 6, the calibration error can be further reduced by the usage of iterative prediction. Both the rotation and translation parts of the calibration parameters have lower calibration errors after multiple iterations than the results without iteration. It can be noted from Table II that after each iteration, the value of most evaluation metrics decreases with the increase of iteration times. However, when the iteration times reaches a certain number, we will find that the calibration error does not go down further, even some parameters go up. The iterative results in Figure

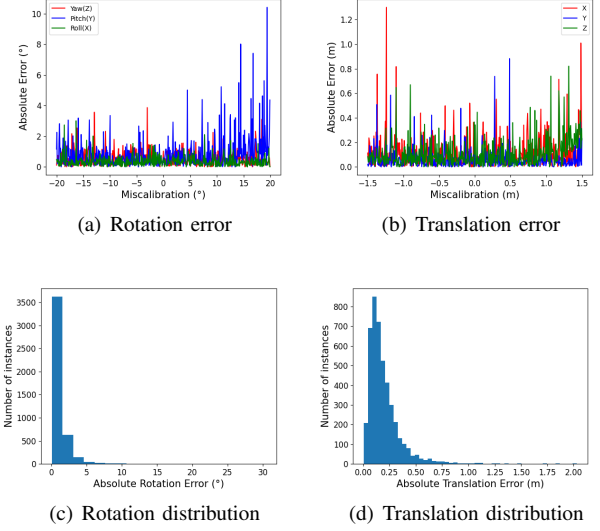


Fig. 4: The error distribution of the predicted extrinsic calibration parameters.

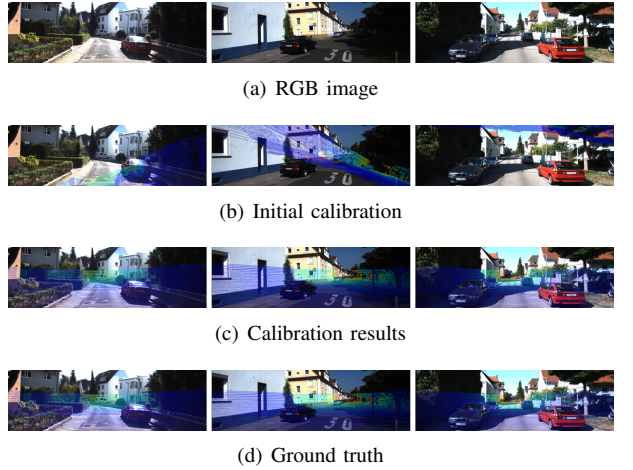


Fig. 5: Example of calibration results for different scenes from the KITTI dataset.

7 also reflect this phenomenon. The main cause of this phenomenon is that each iteration adopts the prediction from the previous iteration to re-project the point clouds and regard the re-projected depth image as a new input of the network. Our network is trained in a large random range, therefore when the deviation reaches a small range, our network cannot further reduce the calibration error. The results of the single-range iteration are described in Table II, our approach achieves a mean square translation error of 10.718cm, a mean translation error of 3.377cm (x, y, z: 2.687cm, 3.804cm, 3.641cm) and a mean quaternion angle error of 0.825°, a mean angle error of 0.498° (roll, pitch, yaw: 0.480°, 0.496°, 0.518°).

(b) The evaluation of a multi-range network.

To solve the problem that single-range network iteration cannot further reduce the calibration error, we use multi-

TABLE I: The results of the absolute extrinsic calibration error

Results of 20°/1.5 m	E_t	Translation (cm)			E_t	Rotation (°)		
		X	Y	Z		Roll	Pitch	Yaw
mean	17.840	11.849	5.169	7.613	1.235	0.170	0.676	0.594
median	13.427	14.415	5.337	4.188	0.898	0.033	0.615	0.549
std.	17.165	5.783	3.847	6.492	1.427	0.260	0.580	0.216

TABLE II: The results of the single-range network iteration

Results of single range 20°/1.5 m		E_t	Translation (cm)			E_R	Rotation (°)		
			X	Y	Z		Roll	Pitch	Yaw
Iteration 1	Mean	17.840	11.849	5.169	7.613	1.235	0.170	0.676	0.594
	Median	13.427	14.415	5.337	4.188	0.898	0.033	0.615	0.549
	Std.	17.165	5.783	3.847	6.492	1.427	0.260	0.580	0.216
Iteration 2	Mean	11.468	3.956	5.136	3.964	0.838	0.568	0.499	0.524
	Median	10.575	3.243	5.833	4.507	0.725	0.486	0.462	0.568
	Std.	5.497	1.586	2.140	1.741	0.500	0.229	0.316	0.111
Iteration 3	Mean	10.723	4.528	1.776	1.547	0.819	0.474	0.576	0.552
	Median	9.825	3.920	1.754	0.323	0.715	0.484	0.579	0.623
	Std.	5.335	2.404	1.777	2.159	0.452	0.386	0.255	0.202
Iteration 4	Mean	10.804	8.695	4.753	4.368	0.817	0.604	0.509	0.484
	Median	9.992	10.827	2.837	2.200	0.722	0.531	0.590	0.613
	Std.	5.349	6.410	5.711	5.412	0.425	0.134	0.327	0.249
Iteration 5	Mean	10.718	2.687	3.804	3.461	0.825	0.480	0.496	0.518
	Median	9.978	0.792	3.470	1.892	0.715	0.461	0.464	0.526
	Std.	5.228	3.402	2.159	3.314	0.467	0.303	0.305	0.273

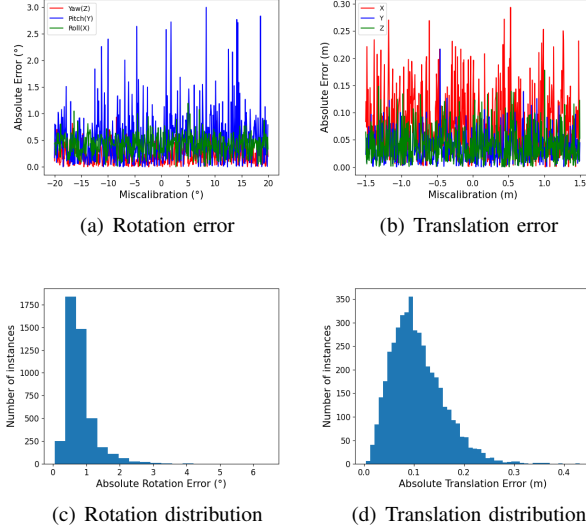


Fig. 6: The error distribution of the predicted extrinsic calibration parameters after single-range iteration.

range network iteration to train the network separately with multiple deviation ranges during the training process. As mentioned in section III-D2(b), we train five different networks with five deviation ranges and iterate these networks in the inference process. The calibration results of the multi-range iterations are shown in Figure 8 and Figure 9. It is obvious that after multi-range iterations, the calibration error is further reduced and the error distribution is concentrated at a smaller value. Different from the results of single-range network iteration, all of

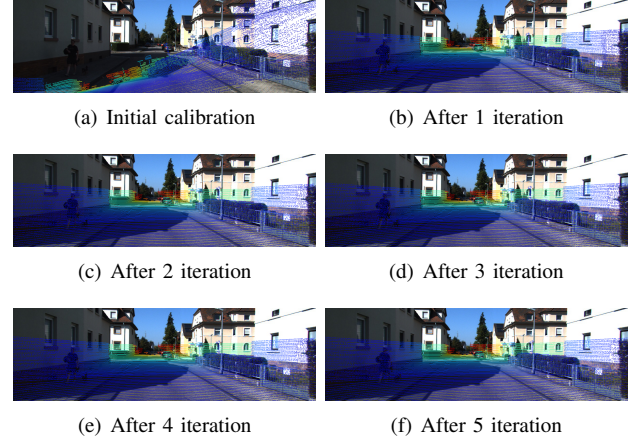


Fig. 7: Iterative prediction of single-range network.

the error evaluation metrics decline after each iteration of multi-range network iteration. The final calibration results of the multi-range iteration are shown in Table III, our approach achieves a mean square translation error of 1.588cm, a mean translation error of 0.361cm (x, y, z: 0.243cm, 0.380cm, 0.459cm), and a mean quaternion angle error of 0.163°, a mean angle error of 0.030° (roll, pitch, yaw: 0.030°, 0.019°, 0.040°).

3) *Temporal Filtering*: In previous experiments, we only exploit a single frame image and LiDAR point cloud to predict the extrinsic calibration parameters. Due to the complexity and changeability of the surrounding environment, illumination changes, moving objects and camera shutter effect will bring the noise to the data collection, resulting in a large error in

TABLE III: The results of the multi-range network iteration

Results of multi-range		E_t	Translation (cm)			E_R	Rotation ($^\circ$)		
			X	Y	Z		Roll	Pitch	Yaw
After $20^\circ/1.5$ m network	Mean	17.834	11.849	5.169	7.613	1.235	0.170	0.676	0.594
	Median	13.423	14.415	5.337	4.188	0.898	0.033	0.615	0.549
	Std.	17.165	5.783	3.847	6.492	1.427	0.260	0.580	0.216
After $10^\circ/1.0$ m network	Mean	6.291	2.045	4.195	2.238	0.594	0.378	0.391	0.405
	Median	5.662	1.929	3.066	2.437	0.452	0.271	0.156	0.218
	Std.	3.494	1.629	3.673	1.683	0.637	0.422	0.480	0.453
After $5^\circ/0.5$ m network	Mean	3.915	1.267	2.212	1.107	0.414	0.309	0.330	0.334
	Median	3.712	1.390	2.410	1.057	0.297	0.028	0.026	0.071
	Std.	0.809	0.686	0.989	0.570	0.541	0.507	0.538	0.479
After $2^\circ/0.2$ m network	Mean	2.069	0.664	0.633	0.281	0.288	0.132	0.103	0.081
	Median	1.592	0.475	0.455	0.316	0.215	0.038	0.040	0.045
	Std.	1.859	0.497	0.581	0.112	0.465	0.196	0.140	0.099
After $1^\circ/0.1$ m network	Mean	1.588	0.243	0.380	0.459	0.163	0.030	0.019	0.040
	Median	1.011	0.262	0.358	0.352	0.121	0.030	0.001	0.022
	Std.	1.776	0.053	0.253	0.254	0.435	0.019	0.031	0.039

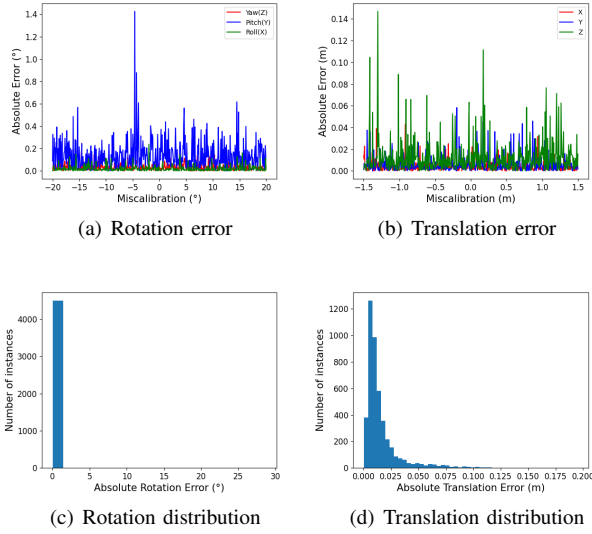


Fig. 8: The error distribution of the predicted extrinsic calibration parameters after multi-range iteration.

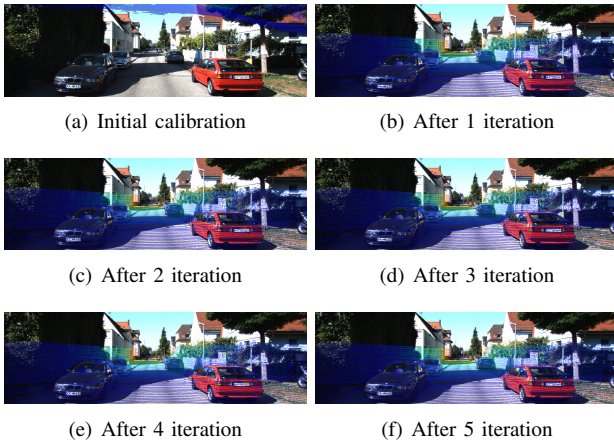


Fig. 9: Iterative prediction of multi-range network.

the prediction of extrinsic parameters. The accuracy of the prediction results can be improved by using the temporal filtering method described in Section III-D3. To verify the validity of the method, we fix the initial parameter T_{init} throughout the sequence and analyze the distribution of the predicted results. The median value of the entire sequence is estimated as the final result. In this experiment, we repeat the operation 100 times in the test dataset. The initial deviation ΔT in each test is randomly sampled within the range of $[-1.5m, 1.5m]$ and $[-20^\circ, 20^\circ]$.

From Figure 10, we can find that our proposed calibration method can accurately predict the extrinsic calibration parameters for different random initial parameters. Although there is a great difference between the two initial parameters shown in Figure 10(a), their corresponding calibration results are almost in full accord. Figure 10(c) also shows that the error distributions of the two tests are very similar. In addition, the proposed method has a high tolerance for the deviation of initial extrinsic parameters, that is the algorithm can perform the calibration task accurately even a few point clouds are projected into the image. The results are exhibited in Table IV, a mean square translation error of 1.010cm, a mean translation error of 0.297cm (x, y, z: 0.262cm, 0.271cm, 0.357cm) and a mean quaternion angle error of 0.122° , a mean angle error of 0.017° (roll, pitch, yaw: 0.020° , 0.012° , 0.019°). The comparison results with other CNN-based extrinsic calibration methods in Table V express that our proposed method is superior to the state-of-the-art.

V. CONCLUSION

In this paper, we proposed a novel deep network for extrinsic calibration of a 3D LiDAR and a 2D camera working in real-time. The calibration network consists of three parts: feature extraction network, feature matching layer, and feature global aggregation network. Compared to other CNN-based approaches, we construct a cost volume between RGB features and depth features for feature matching instead of concatenating these two features directly.

To deal with the scarcity of training data, we add a random deviation to the extrinsic transformation matrix. Therefore,

TABLE IV: The results of the calibration error with temporal filtering

Results	E_t	Translation (cm)			E_t	Rotation ($^\circ$)		
		X	Y	Z		Roll	Pitch	Yaw
Mean	1.010	0.262	0.271	0.357	0.122	0.020	0.012	0.019
Median	1.010	0.260	0.274	0.337	0.122	0.020	0.010	0.019
Std.	0.007	0.087	0.109	0.148	0.001	0.008	0.007	0.009

TABLE V: Comparison results with other CNN-based calibration algorithms.

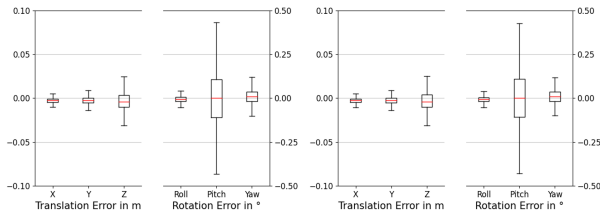
Method	Mis-calibrated range	Translation absolute Error (cm)				Rotation absolute Error ($^\circ$)			
		mean	X	Y	Z	mean	Roll	Pitch	Yaw
Regnet [18]	$[-1.5m, 1.5m]/[-20^\circ, 20^\circ]$	6	7	7	4	0.28	0.24	0.25	0.36
Calibnet [19]	$[-0.2m, 0.2m]/[-10^\circ, 10^\circ]$	4.34	4.2	1.6	7.22	0.41	0.18	0.9	0.15
Ours	$[-1.5m, 1.5m]/[-20^\circ, 20^\circ]$	0.297	0.262	0.271	0.357	0.017	0.020	0.012	0.019



(a) Initial Calibration

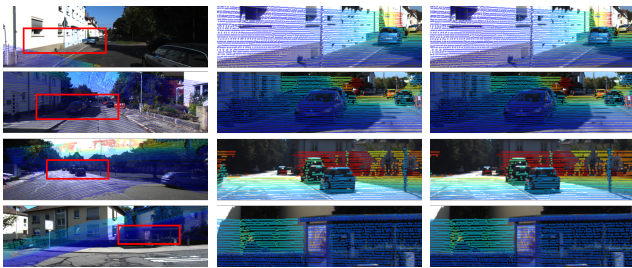


(b) Calibration results



(c) Calibration error with temporal filtering

Fig. 10: Examples of the error distribution for a miscalibration, which is fixed over the test sequence. Five networks are executed iteratively ($20^\circ/1.5m, 10^\circ/1.0m, 5^\circ/0.5m, 2^\circ/0.2m, 1^\circ/0.1m$).



(a)

(b)

(c)

Fig. 11: Results of different single-shot calibration results on the test dataset. (a) Initial Calibration, (b) Ground truth, (c) Calibration results.

the network does not predict the extrinsic calibration between LiDAR and camera directly, but the random deviation. Besides the supervision of the calibration ground truth, we also add a point cloud constrain to the loss function. Iteratively refinement with multiple networks on different decalibration ranges and temporal filtering method is applied to decrease the calibration error. Our method achieves a mean absolute calibration error of $0.297cm$ in translation and 0.017° in rotation with decalibration magnitudes of up to $\pm 1.5m$ and $\pm 20^\circ$, which is superior to other state-of-the-art CNN-based methods.

REFERENCES

- [1] Ganhua Li, Yunhui Liu, Li Dong, Xuanping Cai, and Dongxiang Zhou. An algorithm for extrinsic parameters calibration of a camera and a laser range finder using line features. In *IEEE/RSJ International Conference on Intelligent Robots and Systems*, 2007.
- [2] A. Geiger, F. Moosmann, Ö. Car, and B. Schuster. Automatic camera and range sensor calibration using a single shot. In *2012 IEEE International Conference on Robotics and Automation*, pages 3936–3943, 2012.
- [3] Yoonsu Park, Seokmin Yun, Chee Won, Kyungeun Cho, Kyhyun Um, and Sungdae Sim. Calibration between color camera and 3d lidar instruments with a polygonal planar board. *Sensors*, 14(3):5333–53, 2014.
- [4] Martin Velás, Michal Španěl, Zdeněk Materna, and Adam Herout. Calibration of rgb camera with velodyne lidar. In *WSCG 2014 Communication Papers Proceedings*, volume 2014, pages 135–144. Union Agency, 2014.
- [5] C. Guindel, J. Beltrán, D. Martín, and F. García. Automatic extrinsic calibration for lidar-stereo vehicle sensor setups. In *2017 IEEE 20th International Conference on Intelligent Transportation Systems (ITSC)*, pages 1–6, 2017.
- [6] Z. Pusztai and L. Hajder. Accurate calibration of lidar-camera systems using ordinary boxes. In *2017 IEEE International Conference on Computer Vision Workshops (ICCVW)*, pages 394–402, 2017.
- [7] Hong Wei Jiao, Shi Qiao Qin, Chun Sheng Hu, and Xing Shu Wang. A new extrinsic calibration method of three-dimensional imaging lidar and camera. *Applied Mechanics and Materials*, 58-60:2194–2199, 2011.
- [8] Faraz M Mirzaei, Dimitrios G Kottas, and Stergios I Roumeliotis. 3d lidar-camera intrinsic and extrinsic calibration: Identifiability and analytical least-squares-based initialization. *International Journal of Robotics Research*, 31(4):452–467, 2012.
- [9] P. Núñez, P. Drews, R. Rocha, and J. Dias. Data fusion calibration for a 3d laser range finder and a camera using inertial data. In *Proc. of 4th European Conf on Mobile Robots*, pages 31–36, 2013.
- [10] Weimin Wang, Ken Sakurada, and Nobuo Kawaguchi. Reflectance Intensity Assisted Automatic and Accurate Extrinsic Calibration of 3D LiDAR and Panoramic Camera Using a Printed Chessboard. *Remote Sensing*, 9(8):851, August 2017.

- [11] Subodh Mishra, Gaurav Pandey, and Srikanth Saripalli. Extrinsic Calibration of a 3D-LIDAR and a Camera. *arXiv e-prints*, page arXiv:2003.01213, March 2020.
- [12] Davide Scaramuzza and Ahad Harati. Extrinsic self calibration of a camera and a 3d laser range finder from natural scenes. In *IEEE International Conference on Intelligent Robots and Systems (IROS 2007, 2007*.
- [13] L. Tamas and Z. Kato. Targetless calibration of a lidar - perspective camera pair. In *2013 IEEE International Conference on Computer Vision Workshops*, pages 668–675, 2013.
- [14] Levente Tamas, Robert Frohlich, and Zoltan Kato. Relative pose estimation and fusion of omnidirectional and lidar cameras. In Lourdes de Agapito, Michael M. Bronstein, and Carsten Rother, editors, *eccv-cvrsuad*, volume 8926, pages 640–651, Zurich, Switzerland, September 2014.
- [15] Gaurav Pandey, James R. McBride, Silvio Savarese, and Ryan M. Eustice. Automatic extrinsic calibration of vision and lidar by maximizing mutual information. *Journal of Field Robotics*, 32(5), 2015.
- [16] Zachary Taylor, Juan Nieto, and David Johnson. *Multi-Modal Sensor Calibration Using a Gradient Orientation Measure*. John Wiley and Sons Ltd., 2015.
- [17] Jaehyeon Kang and Nakju L. Doh. Automatic targetless camera-lidar calibration by aligning edge with gaussian mixture model. *Journal of Robotic Systems*, 37(1):158–179, 2020.
- [18] N. Schneider, F. Piewak, C. Stiller, and U. Franke. Regnet: Multimodal sensor registration using deep neural networks. In *2017 IEEE Intelligent Vehicles Symposium (IV)*, pages 1803–1810, 2017.
- [19] Ganesh Iyer, R. Karnik Ram., J. Krishna Murthy, and K. Madhava Krishna. CalibNet: Geometrically Supervised Extrinsic Calibration using 3D Spatial Transformer Networks. *arXiv e-prints*, page arXiv:1803.08181, March 2018.
- [20] Weimin Wang, Shohei Nobuhara, Ryosuke Nakamura, and Ken Sakurada. SOIC: Semantic Online Initialization and Calibration for LiDAR and Camera. *arXiv e-prints*, page arXiv:2003.04260, March 2020.
- [21] Y. Zhu, C. Li, and Y. Zhang. Online camera-lidar calibration with sensor semantic information. In *2020 IEEE International Conference on Robotics and Automation (ICRA)*, pages 4970–4976, 2020.
- [22] Deqing Sun, Xiaodong Yang, Ming-Yu Liu, and Jan Kautz. PWC-Net: CNNs for optical flow using pyramid, warping, and cost volume. 2018.
- [23] Andreas Geiger, Philip Lenz, and Raquel Urtasun. Are we ready for autonomous driving? the kitti vision benchmark suite. In *Conference on Computer Vision and Pattern Recognition (CVPR)*, 2012.